Ultimate strength of RHS T-joints under static compression branch force

M.M. El-Heweity, M.A.F. Diwan, L.M. El-Hifnawy and M.R. Shehata
Dept. of Structural Eng., Faculty of Eng., Alexandria University, Alexandria, Egypt.

In this paper, a theoretical model is presented for the analysis of uni-planar rectangular hollow section (RHS) T-joints under an axial force, P, acting through the branch member. The finite element computer program COSMOS/M is used to determine both of the ultimate and the yield load carrying capacity of the RHS T-joint. The results calculated by the proposed model, taking into consideration the effect of the geometrical parameters of the joints, are compared with those obtained experimentally by the researchers and theoretically with the plastic mechanism models. Also, the results are presented in the form of P-δ curves to determine the modes of failure that occurred in the examined joints. Depending on the results of the proposed model, a verification of modes of failure is performed in order to determine the limits of the geometrical parameters of the joint at which the failure mode changes from a certain failure mode to another.

في هذا البحث، تم تقديم نموذج نظرى لتحليل وصلة T مكونة من قطاعات مستطيلة مفرغة تحت تأثير قوة محورية تؤثر في الضلع الرأسي للوصلة. تم استخدام برنامج العناصر المحددة COSMOS/M لحساب كل من حملي الخضوع والانهيار للوصلة. تم مقارنة النتائج التى تم حسابها من النموذج المقترح أخذين فى الاعتبار تأثير الخواص الهندسية للوصلة مع النتائج المعملية التى قدمها باحثون سابقون وكذلك النتائج النظرية المعتمدة على نماذج ميكانيزم اللدونة. كذلك تم تقديم النتائج في صورة علاقة بين الحمل والهبوط لتعيين أشكال الانهيار التى حدثت فى الوصلات المختبرة. اعتمادا" على نتائج النموذج المقترح، تم التحقق من أشكال الانهيار التى حدثت لتعيين حدود الخواص الهندسية للوصلة والتي عن طريقها يمكن أن تتغير أشكال الانهيار من شكل الي آخر.

Keywords: Rectangular hollow sections, T-joint, Finite element, Ultimate capacity, Failure modes

1. Introduction

The ultimate strength of T-joints is the main aim in the research in the field of T-joints constructed from rectangular hollow sections. There is a considerable amount of research work done in this field in order to estimate the ultimate capacity of the T-joints theoretically and experimentally.

In Japan, Kato et al. [1] performed a series of tests on welded T-joints made of rectangular or square hollow sections. From these tests, three dominating failure modes were recognized. The three dominating failure modes are chord web failure, M_1; chord flange failure, M_2; and local buckling of branch member, M_3. Also in these tests, two combined failure modes were determined namely combined mode of web-crippling and flange yielding of chord, M4; and combined mode of flange yielding of chord and local buckling of branch, M5. The research work performed by Kato et al. [1] has proved that the change of failure mode depends on the distance between surfaces of webs of the chord and the branch members (called eccentricity e).

In Australia, Zhao et al. [2 - 3] examined experimentally a series of tests on cold-formed RHS T-joints. In these tests, a verification of the deformation limit given by Lu et al. [4] was done. The ultimate capacity of the joint is defined by Lu et al. [4] as the following:

- For a joint which has a peak load at a deformation smaller than 3%B (i.e. 3% the chord width) the peak load is considered to be the ultimate load. While, for a joint which has a peak load at a deformation limit greater than 3%B the ultimate load is taken at the deformation limit 3%B.
- For a joint with no peak load, the ultimate capacity of the joint depends mainly on the ultimate deformation limit. In this case, the load is calculated twice at two deformation limits. One at deformation 3%B and the other at 1%B. If the ratio between the loads is greater than 1.5, the deformation limit is 1%B

and if the ratio is less than 1.5, the ultimate deformation limit is 3%B.

The design capacity of RHS T-joints is based mainly on a yield line mechanism for RHS T-joint. Five types of plastic mechanism models are used in predicting the capacity of the joint namely CIDECT model [5], Kato model [1], modified Kato model [6], Monty model [7] and Zhao model [8]. For the first four mechanisms, the capacity of the RHS T-joint is based on a yield line mechanism in the RHS chord flange. While for the last mechanism, the capacity of the joint is based on a yield line mechanism in both the flange and the web of the chord member. The capacity of T-joints calculated from the previous models can be used for failure modes M_2, M_4, M_5 (i.e. chord flange yielding mode, combined mode of chord flange yielding with web crippling, and combined mode of chord flange yielding with buckling of branch member respectively). For T-joints with web crippling failure mode, several formulae are given to calculate the ultimate capacity of the joint namely CIDECT formula [5], AWS formula [9], Packer formula [10] and Zhang et al. formula [11].

2. The model

In order to carry out this research, the finite element program COSMOS/M [12] is employed. The main features of modeling the joint by this program are summarized as follows:

- The behavior of the T-joint is simulated by a three-dimensional model.
- A simple four nodded quadrilateral thick shell element is used.
- In order to separate the influence of bending moment acting on the chord member from the vertical force applied to the branch member, two supports are placed at both ends of the chord member to force zero moments at the ends of the chord member (i.e. the ends of the chord member are simply supported).
- The elements at the ends of both the branch member and chord member are very stiff compared with the rest of elements. Hence, a typical beam-column type of stress distribution has been assumed.
- The branch member is assumed to move vertically only and prevented from rotational or horizontal displacement. The height of the branch member of the joint, H_b, is taken equal to the maximum of either 3h (three times the depth of the branch member) or 3b (three times the width of the branch member)[1].
- Because of symmetry, one quarter of the joint is used in the analysis performed in this research work.
- The model takes into account the effect of the over-all-bending and the in-plane action in the chord member, the size of weld, the material non-linearity and the geometrical non-linearity.
- To predict the elastic strain-hardening behavior of the RHS T-joint, twenty-seven integration points are used for a bi-linear stress-strain curve for steel.
- The loads are applied in an incremental manner using the modified Newton-Raphson technique. The displacement control technique is used to pass the limit point and to trace the behavior of the joints in the post-plastic stage

Fig. 1 shows the finite element mesh for quarter of the joint with boundary conditions and applied load.

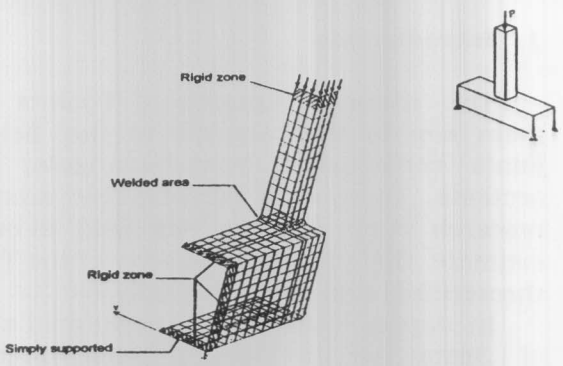

Fig. 1. Finite element mesh for quarter of T-joint under branch compressive force.

3. Parametric study

In this study, 15 joints experimented in Japan by Kato et al. [1] and 5 joints experimented in Australia by Zhao and Hancock [2] have been analyzed under axial force, P, acted through the branch member of the joint. The joints specified for the parametric study cover all types of failure

modes discussed by Kato et al. [1]. The geometrical parameters of the joints such as the width ratio, β, width to thickness ratio of the chord, 2γ, and thickness of the branch member to that of the chord member, τ, are varied to evaluate the effect of the geometrical parameters on changing the failure mode of the joint. The variation of these geometrical parameters is from 0.3 to 1.0, 10-50, and 0.18 to 2.65 respectively. For modes of failure M2, M4, and M5 (i.e. modes of failure having a chord flange failure), the results obtained from the proposed model are compared with the plastic mechanism models mentioned in the introduction. Also, for mode of failure M1 (i.e. web crippling failure mode) the results are compared with the design formulae used to predict the ultimate capacity of the joint in case of web crippling. The static behavior of the T-joints, i.e. the yield load, and the ultimate load of the joints, has been calculated. Also, the load at certain deformation limits is calculated in order to evaluate the capacity of the joint that satisfies the ultimate deformation limits. The maximum deformation in the chord wall is calculated in case of web crippling failure mode and also estimated in the other failure modes but corresponding to a deformation limit equal to 3% B.

3.1. Characteristics of the joints used

The nominal dimensions, the yield stresses and the ultimate stresses of the T-joints analyzed in this study are tabulated in table 1 for the T-joints tested in Japan and Australia. The table includes for each joint: the dimensions of both the chord and the branch members; the ratio of the width of the branch to that of the chord, β; the ratio of the width of the chord to the thickness of the chord, 2γ; the length of the chord member,

Table 1
Dimensions of T-joints used

i) T-Joints in Japan [1]

No. of joint	Dimensions of chord member (mm)			Dimensions of branch member (mm)			β	2γ	L (mm)	h_b (mm)	Stresses in chord member (kN/mm²)		Stresses in branch member (kN/mm²)	
	B	H	t	b	h	t_1					σ_y	σ_u	σ_y	σ_u
Kato 4	127	127	3.0	102	102	6.4	0.80	42.33	356	306	382	469	431	486
Kato 11	150	150	6.0	100	100	6.0	0.67	25.00	400	300	366	431	424	492
Kato 13	250	250	6.0	200	200	9.0	0.80	41.67	700	600	400	490	414	466
Kato 16	150	150	6.0	75	75	3.2	0.50	25.00	375	225	366	431	390	471
Kato 21	254	254	9.5	127	127	6.4	0.50	26.74	635	381	380	481	446	505
Kato 22	178	178	12.7	127	127	6.4	0.71	14.00	483	381	380	446	446	505
Kato 26	150	150	6.0	75	75	2.3	0.50	25.00	375	225	366	431	358	445
Kato 27	150	150	6.0	102	102	3.2	0.68	25.00	402	306	366	431	393	456
Kato 28	127	127	7.9	102	102	3.2	0.80	16.00	356	306	404	453	393	456
Kato 32	350	350	12.0	102	102	2.4	0.29	29.17	802	306	264	409	369	453
Kato 33	254	254	9.5	127	127	3.0	0.50	26.74	635	381	380	481	343	450
Kato 34	178	178	12.7	127	127	3.0	0.71	14.00	483	381	380	446	343	450
Kato 35	127	127	7.9	102	102	2.4	0.80	16.00	356	306	404	453	369	453
Kato 40	350	350	12.0	102	102	2.1	0.29	29.17	802	306	264	409	366	452
Kato 42	150	150	6.0	102	102	2.1	0.68	25.00	402	306	366	431	366	452

ii) T-joints in Australia [2]

No. of joint	Dimensions of chord member (mm)			Dimensions of branch member (mm)			β	2γ	L (mm)	h_b (mm)	Stresses in chord member (kN/mm²)		Stresses in branch member (kN/mm²)	
	B	H	t	b	h	t_1					σ_y	σ_u	σ_y	σ_u
S1B1C11	102	51	4.9	51	51	4.9	1.00	10.4	800	200	379	418	379	418
S1B1C12	102	51	3.2	51	51	4.9	1.00	15.9	800	200	330	431	330	431
S1B1C13	102	51	2.0	51	51	4.9	1.00	25.5	800	200	400	467	400	467
S1B2C21	102	102	9.5	102	102	8.0	1.00	10.7	800	200	421	454	421	454
S1B2C22	102	102	6.3	102	102	8.0	1.00	16.2	800	200	412	455	412	455

L; the height of the branch member, h_b; and the measured yield and ultimate stresses for the chord member and the branch member.

3. Numerical results

The results of the proposed model are given in table 2. The table lists: the yield load, P_y, the ultimate load, P_u, the load at a deformation limit of the chord flange equals 1%B, $P_{1\%B}$, the load at a deformation limit of the chord flange equals 3%B, $P_{3\%B}$, and the type of failure mode. Typical graphs are plotted between the load and the centerline deflection of the top flange of the chord member for both experimental and theoretical results in order to examine the model in tracing the behavior of the joints in all modes of failure. In the following subsections, the numerical results obtained are compared with the test results of the joints done by Kato et al. [1] and Zhao et al. [2] and with the existing formulae mentioned above.

Table 2
Numerical results of T-joints

No. of joint	Proposed model results in (kN)				
	P_y	P_u	$P_{1\%B}$	$P_{3\%B}$	Failure mode
Kato 4	-	85.00	66.05	83.92	M4
Kato 11	160.00	217.00	143.50	188.11	M2
Kato 13	-	270.00	222.05	270.00	M4
Kato 16	104.26	184.55	79.13	114.00	M2
Kato 21	215.00	420.12	181.05	275.16	M2
Kato 22	-	952.4	650.13	950.5	M4
Kato 26	103.72	138.00	73.99	108.74	M2
Kato 27	161.00	216.10	136.22	177.24	M2
Kato 28	-	384.37	-	-	M3
Kato 32	164.00	211.85	121.49	211.85	M5
Kato 33	227.07	340.23	153.17	255.07	M2
Kato 34	-	440.00	-	-	M3
Kato 35	-	215.00	-	-	M3
Kato 40	160.00	185.00	110.39	179.00	M5
Kato 42	150.00	178.16	120.20	159.35	M5
S1B1C11	-	300.00	-	300.00	M1
S1B1C12	-	150.10	-	-	M1
S1B1C13	-	74.23	-	-	M1
S1B2C21	-	1100.0	-	1070.0	M1
S1B2C22	-	615.00	-	-	M1

4.1. Web crippling failure mode

Table 3 shows the values of the maximum load calculated by the model presented and those obtained experimentally in Australia. Also, the corresponding deflections at the top flange of the chord member in the two cases are tabulated in order to determine the ultimate capacity of the joint. From the results given in table 3, it can be seen that the numerical results obtained by using the proposed model are in good agreement with those obtained experimentally in Australia. The ultimate capacity of the T-joints is lower than the experimental results by about 6.5% with coefficient of variation equals 0.0349.

Figs. 2- 6 show the load versus centerline deflection of the joints in case of web crippling failure mode. From these figures, good agreement with the experimental results is obtained. Also, one can notice that the failure of the joint in case of the theoretical model results occurs in a stage earlier than the experimental ones. This is because the failure of the joint in case of the theoretical analysis is defined as the load which gives the first ultimate stress on the joint while in the experimental analysis the failure of the joint occurs when much number of plastic hinges are formed in the joint.

4.2. Chord flange failure mode

Table 4 lists the values of the yield load and the ultimate load of the joints calculated by the model used and those obtained experimentally in Japan. The loads at deformation limits 1%B and 3%B are also calculated

Table 3
Comparisons between the theoretical results obtained and the experimental results for failure mode M1

No. of joint	Theoretical results			Experimental results			
	P_{max} (kN)	Δw_{max} (%B)	P_{cap} (kN)	$P_{(max)exp}$ (kN)	$\Delta w_{(max)exp}$ (%B)	$P_{(cap)exp}$ (kN)	$P_{cap}/P_{(cap)exp}$
S1B1C11	300.00	3.00	300.00	326.00	3.14	324.00	0.9259
S1B1C12	150.10	2.10	150.10	163.00	2.25	163.00	0.9209
S1B1C13	74.23	2.10	74.23	75.40	2.31	75.40	0.9845
S1B2C21	1100.00	3.50	1070.00	1207.00	4.08	1193.00	0.8969
S1B2C22	615.00	2.11	615.00	652.00	2.33	652.00	0.9433
Mean	-	-	-	-	-	-	0.9343
Cov.	-	-	-	-	-	-	0.0349

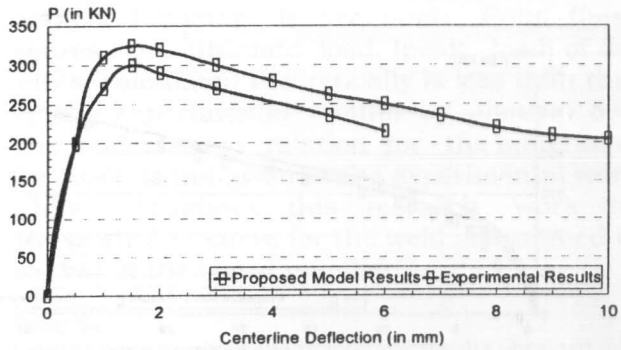

Fig. 2. Load versus flange deflection curve for joints S1B1C11(failure mode M1).

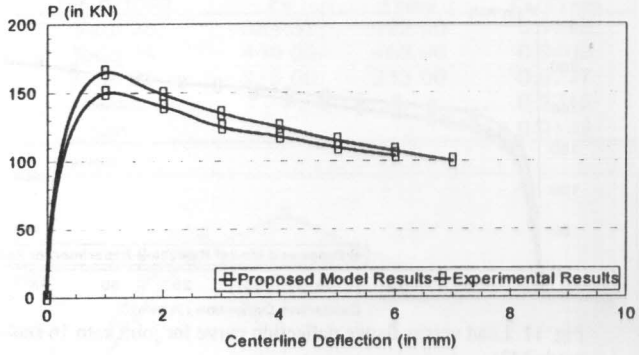

Fig. 3. Load versus flange deflection curve for joint S1B1C12 (failure mode M1).

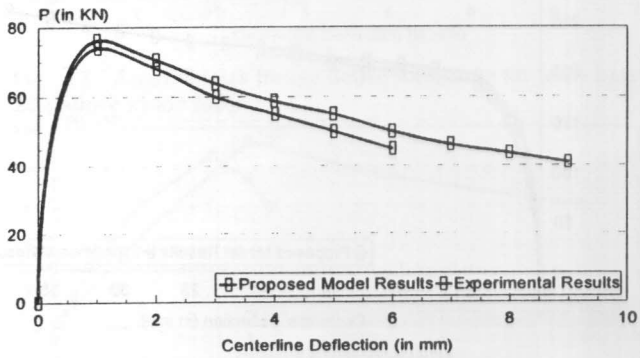

Fig. 4. Load versus flange deflection curve for joint S1B1C13 (failure mode M1).

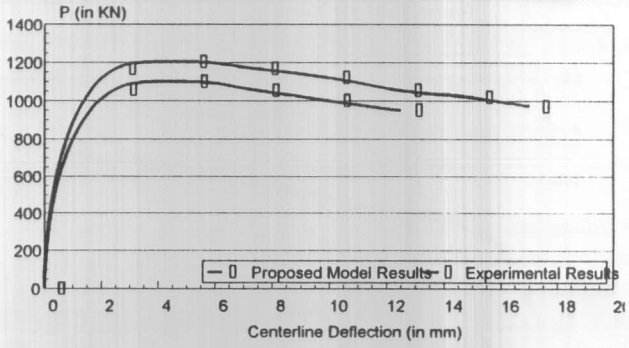

Fig. 5. Load versus flange deflection curve for joint S1B2C21 (failure mode M1).

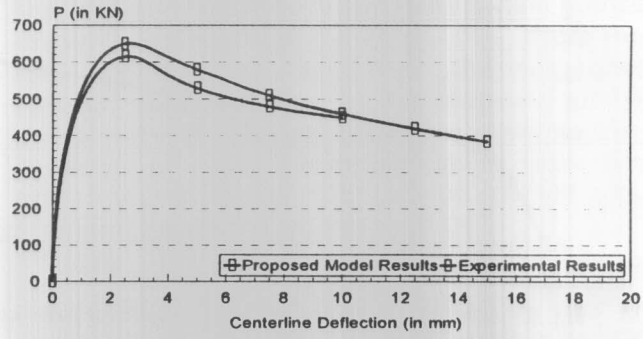

Fig. 6. Load flange deflection curve for joint S1B2C22 (failure mode M1).

and tabulated in order to determine the ultimate capacity of the joint. From table 4, it can be seen that the capacity of T-joints under axial force is lower than the experimental results by about 5% with coefficient of variation equals 0.1628.

Figs. 7-12 show the load versus centerline deflection of the joints in case of chord flange failure mode. It can be seen from the figures that the ultimate load obtained by the theoretical model is lower than that of the experimental results by approximately 15%.

Table 4
Comparisons between the theoretical results obtained and the experimental results for failure mode M2

No. of Joint	$P_y / P_{(y)exp}$	$P_u / P_{(u)exp}$	$P_{1\%B} / P_{(1\%B)exp}$	$P_{3\%B} / P_{(3\%B)exp}$	$P_{cap} / P_{(cap)exp}$
Kato 11	0.8333	0.8411	0.8969	0.9647	0.9647
Kato 16	1.0221	0.8873	1.0607	1.0088	1.0088
Kato 21	0.8175	0.8206	0.8919	0.8992	0.8919
Kato 26	1.1033	0.7931	1.1507	1.0456	1.0456
Kato 27	0.8519	0.8542	0.8514	0.9183	0.9183
Kato 33	0.9193	0.8548	0.8703	0.9142	0.8703
Mean	0.9246	0.8419	0.9537	0.9585	0.9499
Cov	0.1244	0.0815	0.2855	0.1355	0.1628

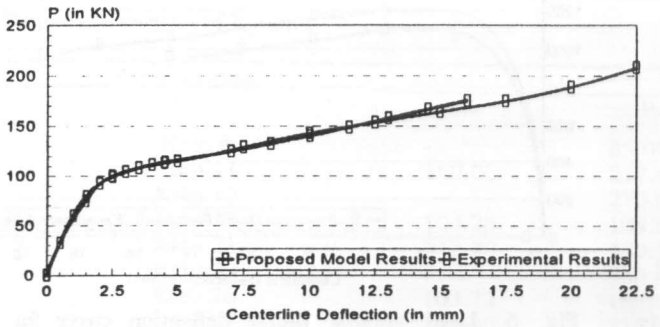

Fig. 7. Load versus flange deflection curve for joint kato 16 (failure mode M2).

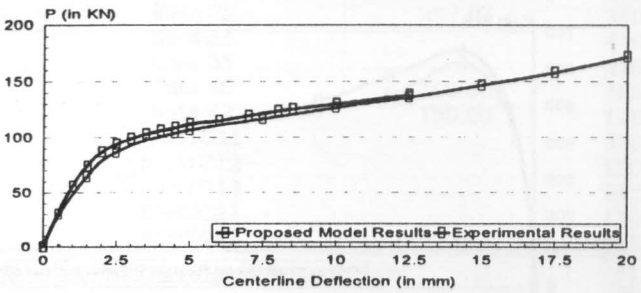

Fig. 8. . Load versus flange deflection curve for joint kato 26 (failure mode M2).

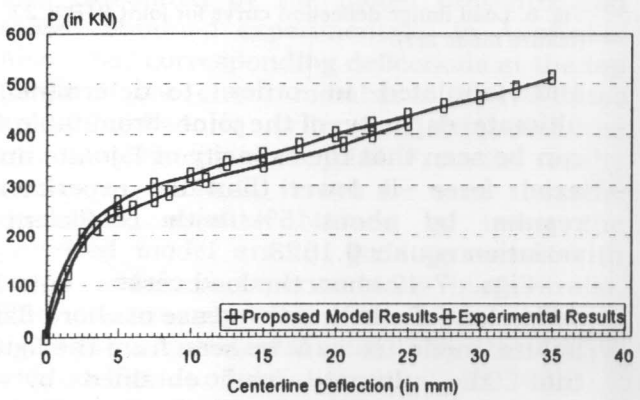

Fig. 9. Load versus flange deflection curve for joint kato 11. (failure mode M2).

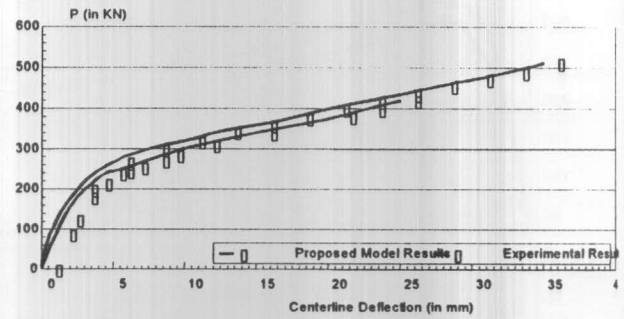

Fig. 10. Load versus flange deflection curve for joint kato 16 (failure mode M2).

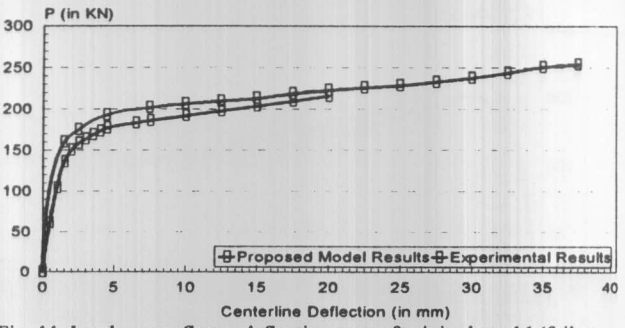

Fig. 11. Load versus flange deflection curve for joint kato 16 (failure mode M2).

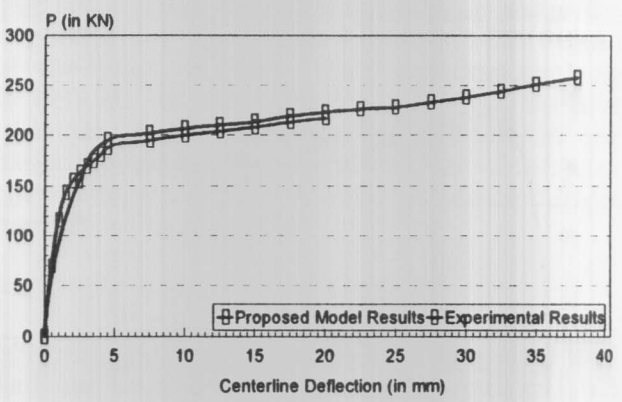

Fig. 12. Load versus flange deflection curve for joint kato 33 (failure mode M2).

4.3. Branch buckling failure mode

Table 5 shows the values of the ultimate load of the joints calculated by the model used and those obtained experimentally in Japan The mean value of the theoretical results, obtained by using the proposed model, is lower than the experimental ones by about 7.5% with coefficient of variation 0.0122.

Figs. 13- 15 show the load versus centerline deflection of the joints in case of branch buckling failure mode. From these figures, the ultimate load (peak load) of the joints calculated theoretically is less than that in the experimental results by about 7.5%. The stress-strain relation for the material of the weld is not given in the experimental work while throughout this research work the stress-strain curve for the weld is assumed to be that of the chord member.

Table 5
Comparisons between the theoretical results obtained and the experimental results for failure mode M3

No. of joint	P_u	$P_{(u)exp}$	$P_u/P_{(u)exp}$
Kato 28	384.37	422.00	0.9108
Kato 34	440.00	468.00	0.9402
Kato 35	215.00	233.00	0.9227
Mean	-	-	0.9246
Cov.	-	-	0.0122

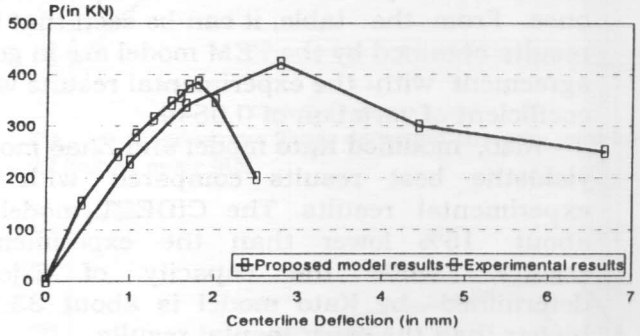

Fig. 13. Load versus flange deflection curve for joint kato 28 (failure mode M3).

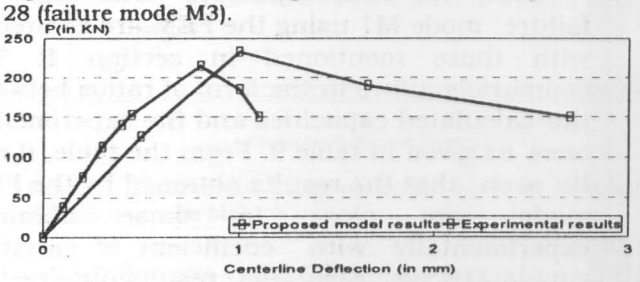

Fig. 14. Load versus flange deflection curve for joint kato 35 (failure mode M3).

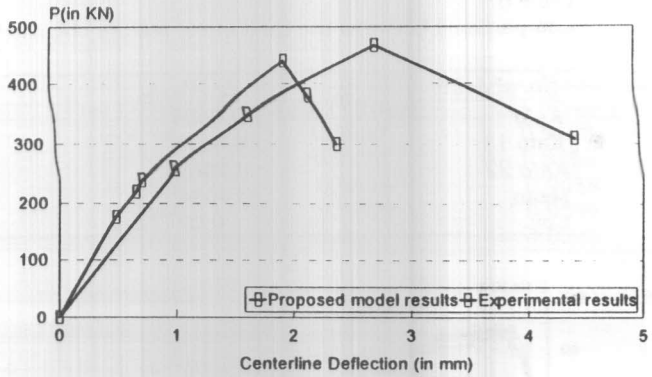

Fig. 15. Load versus flange deflection curve for joint kato 34 (failure mode M3).

4.4. Combined failure mode between web crippling and chord flange failure

Table 6 shows the values of the maximum load of the joint calculated by the model used and those obtained experimentally in Japan. The loads at deformation limits 1%B and 3%B are also calculated and tabulated in order to determine the capacity of the joint. The ultimate deformation limit corresponding to the ultimate capacity of the joint in this failure mode is defined by Lu et al. [4]. From the table, it can be seen that the numerical results obtained by using the proposed model are close to the experimental results. The capacity of the T-joints is lower than the experimental ones by about 6.7% with coefficient of variation equals 0.045.

Figs. 16-18 show the load versus centerline deflection of the joints in case of combined failure mode between web crippling and chord flange failure. From these figures, it is clear that the load carrying capacity continues to keep its level after web crippling took place due to the effect of the membrane action of the flange.

4.5. Combined failure mode between chord flange failure and branch buckling failure

Table 7 lists the values of the yield load and the ultimate load of the joints evaluated by the model and those obtained experimentally in Japan. The loads at deformation limits 1%B and 3%B are also calculated and tabulated in order to determine

Table 6
Comparisons between the theoretical results obtained and the experimental results for failure mode M4

No. of Joint	$P_u / P_{(u)exp}$	$P_{1\%B} / P_{(1\%B)exp}$	$P_{3\%B} / P_{(3\%B)exp}$	$P_{cap} / P_{(cap)exp}$
Kato 4	0.9659	0.8889	0.9092	0.9092
Kato 13	0.9375	0.9063	0.9091	0.9091
Kato 22	0.9869	0.9377	0.9799	0.9799
Mean	0.9634	0.9110	0.9327	0.9327
Cov.	0.0277	0.0250	0.0450	0.0450

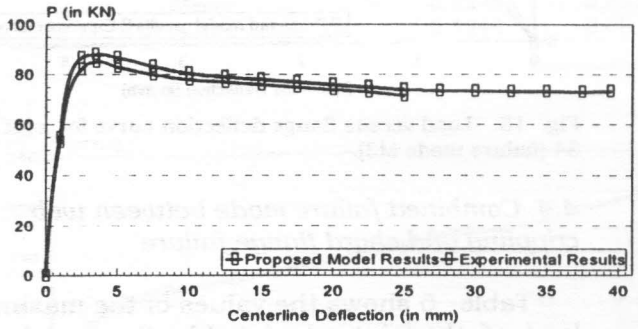

Fig. 16. Load versus flange deflection curve for joint kato 4 (failure mode M4).

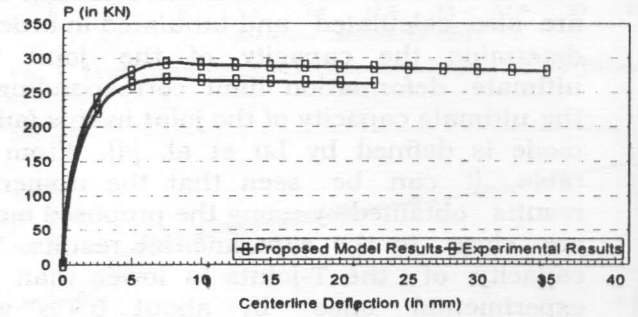

Fig. 17. Load versus flange deflection curve for joint kato 13 (failure mode M4).

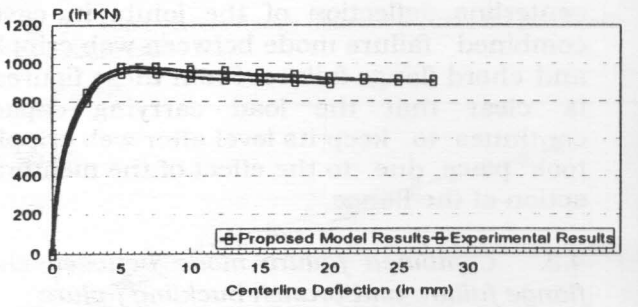

Fig. 18. Load versus flange deflection curve for joint kato 22 (failure mode M4).

the capacity of the joint. The ultimate deformation limit corresponding to the ultimate capacity of the joint in this failure mode is that defined before by Lu et al. [4].

From the table, it can be seen that the ultimate capacity of T-joints is lower than the experimental results by about 4% with coefficient of variation equals 0.0228.

Figs. 19-21 show the load versus centerline deflection of the joints in case of combined failure mode between chord flange failure and branch buckling failure. It is clear that the local buckling of the branch member takes place after some amount of plastic deformation due to the yielding of the chord flange.

4.6. Comparison with the design formulae

The load capacities determined for failure modes M2, M4 and M5 using the FEM are compared with those mentioned in the introduction. The comparisons are given in table 8 in the form of ratios between the calculated capacities and the experimental ones. From the table, it can be seen that the results obtained by the FEM model are in good agreement with the experimental results with coefficient of variation of 0.0549.

Also, modified Kato model and Zhao model yieldsthe best results compared with the experimental results. The CIDECT model is about 15% lower than the experimental results, while the capacity of T-joint determined by Kato model is about 33.7% higher than the experimental results.

Also, the load capacities determined for failure mode M1 using the FEM are compared with those mentioned in section 1. The comparisons are in the form of ratios between the calculated capacities and the experimental ones as given in table 9. From the table, it can be seen that the results obtained by the FEM model are close to those obtained experimentally with coefficient of variation equals 0.0349. Also, the results obtained by Zhang et al. and Packer are about 15% lower than the experimental results.

Table 7
Comparisons between the theoretical results obtained and the experimental results for failure mode M5

No. of Joint	$P_y / P_{(y)exp}$	$P_u / P_{(u)exp}$	$P_{1\%B} / P_{(1\%B)exp}$	$P_{3\%B} / P_{(3\%B)exp}$	$P_{cap} / P_{(cap)exp}$
Kato 32	0.9535	0.8754	0.9798	0.9899	0.9798
Kato 40	0.9039	0.8894	0.9331	0.9728	0.9331
Kato 42	0.9317	1.0298	0.9465	0.9658	0.9658
Mean	0.9297	0.9315	0.9531	0.9762	0.9596
Cov.	0.0267	0.0923	0.0272	0.0077	0.0228

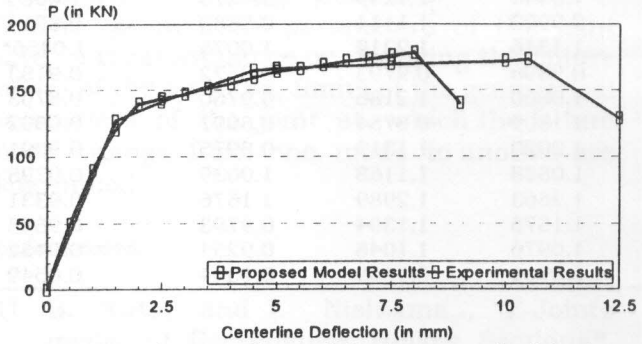

Fig. 19. Load versus flange deflection curve for joint kato 42 (failure mode M5).

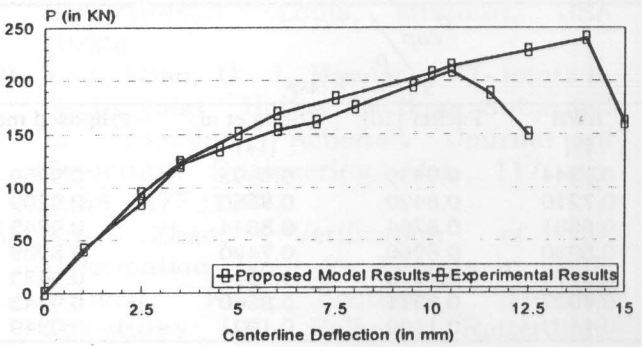

Fig. 20. Load versus flange deflection curve for joint kato 32 (failure mode M5).

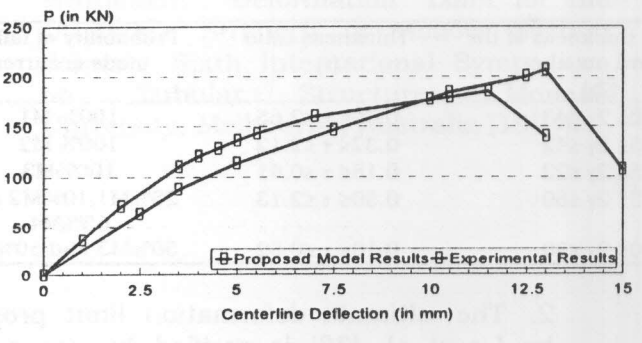

Fig. 21. Load versus flange deflection curve for joint kato 40 (failure mode M5).

While, the CIDECT design formula and the AWS design formula are about 35% and 30% respectively lower than the experimental results.

4.7. Geometrical effect on the failure modes of the joints

From the numerical results obtained, the failure modes of the joint change by changing the geometrical parameters of the joint (i.e. width ratio, β, width to thickness of the chord member, 2γ, and thickness ratio, τ).

Table 10 gives the ranges of the geometrical parameters of the joint corresponding to each failure mode.

As seen from the table, the influence of the parameter τ on changing the failure modes is clearly observed for modes of failure M3, M4, and M5. This parameter has not been taken into consideration in Kato experimental analysis [1] who focused on the effect of the eccentricity, e, on changing the failure mode and neglected the effect of both 2γ and τ. From the present results, the following observations may be stated:

- Failure modes M1 and M2 depends mainly on the width ratio of the joint, β. This agrees with the fact that failure mode M1 (i.e. web crippling failure mode) occurs at large width ratio (i.e. $\beta \geq 0.80$) and failure mode M2 (i.e. chord flange failure mode) occurs at medium width ratio (i.e. $0.30 \leq \beta \leq 0.70$).
- Failure mode M3 depends on the thickness ratio between the branch member and the chord member. For small thickness ratio (i.e. $\tau \leq 0.4$) buckling of the branch member occurs.
- For failure mode M4, the geometrical parameters can not distinguish exactly the failure mode since this failure mode is a combination between two failure modes. From the results obtained, the width ratio is the control geometrical parameter for $0.70 < \beta < 0.80$.

Table 8
Comparisons between the theoretical results obtained and the design formulae for failure modes M2, M4and M5

No. of joint	$P_{cap}/P_{(cap)_{exp}}$					
	Cidect [5]	Kato [1]	Modified Kato [6]	Zhao [8]	Mouty [7]	Proposed model
Kato 11	0.7385	1.1795	0.9333	0.9333	0.7961	0.9647
Kato 16	0.8938	1.1593	1.0443	1.1239	0.9273	1.0088
Kato 21	0.8595	1.0882	0.9902	1.1111	0.8889	0.8919
Kato 26	0.9712	1.2596	1.1346	1.2212	1.0075	1.0456*
Kato 27	0.7720	1.2746	0.9896	0.9793	0.8372	0.9183
Kato 33	0.9427	1.1935	1.0860	1.2186	0.9750	0.8703
Kato 4	0.6392	1.9393	1.1809	0.8754	0.6991	0.9092
Kato 13	0.8215	1.6801	1.2020	1.1313	0.8975	0.9091
Kato 32	0.9907	1.1308	1.0888	1.1168	1.0039	0.9798
Kato 40	1.1522	1.3098	1.2663	1.2989	1.1676	0.9331
Kato 42	0.9030	1.4909	1.1576	1.1394	0.9793	0.9658
Mean	0.8804	1.3368	1.0976	1.1045	0.9254	0.9452
Cov.	0.1577	0.1977	0.0931	0.1159	0.1344	0.0549

Table 9
Comparisons between the theoretical results obtained and the design formulae for failure mode M1

No. of joint	$P_{cap}/P_{(cap)_{exp}}$				
	CIDECT [5]	AWS [9]	Packer [10]	Zhang et al. [11]	Proposed model
S1B2C21	0.7649	0.7244	0.9439	0.9095	0.9259
S1B2C22	0.8350	0.7210	0.8420	0.9560	0.9209
S1B1C11	0.8110	0.6681	0.8764	0.8844	0.9845
S1B1C12	0.5600	0.5930	0.6960	0.7490	0.8969
S1B1C13	0.2700	0.8070	0.7970	0.7810	0.9433
Mean	0.6482	0.7027	0.8311	0.8560	0.9343
Cov.	0.3665	0.1123	0.1109	0.1021	0.0349

Table 10
Validity ranges of the geometrical parameters for each failure mode

Failure mode (M)	Width ratio (β)	Width to thickness of the chord member (2γ)	Thickness ratio (τ)	Probability of failure mode occurred
M1	$0.80 \le \beta \le 1.0$	$10 \le 2\gamma \le 43$	$0.50 \le \tau \le 2.65$	100% M1
M2	$0.30 \le \beta \le 0.70$	$15 \le 2\gamma \le 42$	$0.32 \le \tau \le 2.12$	100% M2
M3	$0.28 \le \beta \le 0.85$	$15 \le 2\gamma \le 22$	$0.18 \le \tau \le 0.41$	100%M3
M4	$0.70 \le \beta \le 0.85$	$15 \le 2\gamma \le 50$	$0.50 \le \tau \le 2.13$	25%M1,10%M2 and 65%M4
M5	$0.28 \le \beta \le 0.75$	$10 \le 2\gamma \le 30$	$0.18 \le \tau \le 0.52$	50%M3 and 50%M5

5. Conclusions

1. The results of the proposed numerical model are in good agreement with the experimental results available in the literature for all modes of failure.
2. The ultimate deformation limit proposed by Lu et al. [38] is verified by comparing it with those obtained from the numerical results.
3. The deformation limits obtained numerically in case of branch compressive force agrees with the experimental results.

While they fail to agree when the combined actions of chord forces and branch force are considered.

4. The ultimate branch axial loads obtained in almost all cases were found to be higher than the corresponding yield load by approximately 1.75. Accordingly, the load at which initial yielding begins is far conservative as a criterion for design purposes.

5. The geometrical parameters of the joint have a great influence on changing the failure mode of the joint. So, limits of the geometrical parameters of the joint at which the failure mode change from one mode to another are determined.

References

[1] B. Kato, and I. Nishiama,., "T-Joints made of Rectangular Hollow Sections". Proceedings, Fifth Int. Specialty Conference on Cold Formed Steel Structures,St. Louis, Missouri, USA (1980).

[2] X. L Zhao, G. J. Hancock, "T-Joints in Rectangular Hollow Sections Subjected to Combined Actions". Journal of Structural Engineering, Vol. 117, pp. 2258-2277 (1991).

[3] X.L. Zhao, "Verification of the Deformation Limit for T-joints in Cold-Formed RHS Sections". Tubular Structures VII, Balkema, Rotterdam, Netherlands (1996).

[4] L. H. Lu, G. D. Winkel, Y. Yu, and J. Wardenier, "Deformation Limit for the Ultimate Strength of Hollow Section Joints". Sixth International Symposium on Tubular Structures, Monash University, Melbourne, Australia (1994).

[5] J. A.. Packer, J. Wardenier, Y. Kurobane, D. Dutta, and N. Yeomans, " Design Guide For Rectangular Hollow Section (R.H.S) Joints Under Predominantly Static Loading". Edited by CIDECT (1992).

[6] X. L Zhao, and , G. J. Hancock, "Plastic Mechanism Analysis of T-Joints in R.H.S Subjected to Combined Bending and Concentrated Force". Journal of Singapore Structural Steel Society, Vol. 2, 1, pp. 31-44 (1993).

[7] J. Mouty, "Theoretical Prediction of Welded Joint Strength". International Symp0osium on Hollow Structural Sections, Toronto Symposium (1977).

[8] X. L Zhao, and G. J. Hancock, "Plastic Mechanism Analysis of T-Joints in R.H.S under Concentrated Force". Journal of Singapore Str. Steel Society, Vol. 2(1), pp. 31-44 (1991).

[9] AWS, "Structural Welding Code-Steel ANSI/AWS D1.1-92". 13th. Edition, American Welding Society Inc., Miami, Fla., USA (1992).

[10] J. Packer, "Web Crippling of Rectangular Hollow Sections" ASCE, Vol. 110(10) (1984).

[11] Z.L Zhang, et al., "Nonlinear FEM Analysis and Experimental Study of ultimate Capacity of Welded RHS Joints". Proc. Int. Symposium on Tubular Structures, Lappeenranta, Finland (1989).

[12]COSMOS/M "A computer program for nonlinear static and dynamic analysis". Structural Research and Analysis Corporation, Santa Monica, California, USA (1993).

Received December 1,2000
Accepted June 30,2001